

Spontaneous four-wave mixing in a thin layer with second-order nonlinearity

CHANGJIN SON^{1,2,*} AND MARIA CHEKHOVA^{1,2}

¹Max Planck Institute for the Science of Light, 91058 Erlangen, Germany

²Friedrich-Alexander Universität Erlangen-Nürnberg, 91058 Erlangen, Germany

*changjin.son@mpl.mpg.de

Compiled February 2, 2026

Pairs of entangled photons are crucial for photonic quantum technologies. The demand for integrability and multi-functionality suggests ‘flat’ platforms - ultrathin layers and metasurfaces - as sources of photon pairs. With the success in demonstrating spontaneous parametric down-conversion (SPDC) from such sources, an alternative process to generate photon pairs, spontaneous four-wave mixing (SFWM), also starts to attract interest. In materials with nonzero second-order nonlinear susceptibility $\chi^{(2)}$, SFWM can generate photon pairs both directly, through the third-order nonlinear susceptibility $\chi^{(3)}$, and in a cascaded way, through second harmonic generation (SHG) followed by SPDC. Usually, the cascaded process is more efficient. Here, we show that in a thin layer, direct SFWM dominates, because the wavevector mismatch for SFWM is much smaller than for SHG or SPDC. To demonstrate it, we implement the photon pair generation via SFWM in a second-order nonlinear material - a thin layer of lithium niobate (LN). The existence of both second- and third-order nonlinear processes offers broader opportunities for quantum state engineering.

<http://dx.doi.org/10.1364/ao.XX.XXXXXX>

1. INTRODUCTION

Spontaneous parametric down-conversion (SPDC) - a second-order nonlinear process where a single pump photon splits into a pair of daughter photons - is widely used to generate entangled photons in bulk crystals and waveguides. During the last few years, SPDC has been also implemented in micro- and nanoscale nonlinear layers [1–12]. Due to their tiny thickness, such layers satisfy the SPDC phase-matching automatically, even though the wavevector mismatch Δk can be very large. As a result, materials with high second-order susceptibility $\chi^{(2)}$, or orienta-

tions using large components of the $\hat{\chi}^{(2)}$ tensor, which normally are excluded from SPDC because of phase-matching restriction, come into play. Although, because of the small thickness, such sources produce photon pairs at low rates - up to a few kHz so far [12, 13] - their advantage is multifunctionality. For example, a thin layer can generate photon pairs not only forwards, but also backwards and bidirectionally [14]; by tuning the pump polarization, the polarization state and the degree of entanglement of the photon pairs can be also tuned [3, 6]; the pump wavelength and direction can be chosen arbitrarily.

The variety of materials used to generate entangled photons through SPDC is quickly expanding. Most promising are van der Waals crystals [4, 6, 8, 10], whose nonlinearity can be controlled by stacking several atomic layers in different ways [15]. Recently, entangled photons were generated in a liquid crystal [13, 16], which offers new ways to control the properties of entangled photons: through molecular orientation twist and by applying electric field.

An alternative way to generate photon pairs is the spontaneous four-wave mixing (SFWM), where two pump photons are converted into a pair of entangled photons and the third-order susceptibility $\chi^{(3)}$ is involved. Since $\chi^{(3)}$ is nonzero in any material, the material choice becomes broader. An important advantage of SFWM is that it generates entangled photons on both sides of the pump spectral line. This allows one of the photons to cover blue or even UV range of wavelengths [17] without using even more blue-shifted pump. During the last few years, considerable efforts to implement SFWM in ‘flat’ sources have been made. However, due to the weakness of the third-order nonlinear interaction compared to the second-order one, most of the experiments on SFWM in thin sources are carried out in the seeded regime [18–22], where a coherent beam at the frequency of one of the output photons is stimulating the process. So far, there are only two experiments on photon pair generation via SFWM in thin layers [23, 24].

Meanwhile, SFWM can also take place in non-centrosymmetric materials, where both $\chi^{(2)}$ and $\chi^{(3)}$ are present. Such materials were so far avoided in SFWM experiments. In the absence of the phase-matching restriction, a direct third-order nonlinear process should compete with a cascaded process. For example, the third harmonic can be generated not only directly but also through the second harmonic generation (SHG) followed by sum frequency generation. This cascaded

process is well-studied, both theoretically and experimentally [25, 26]. Similarly, both cascaded and direct nonlinear processes can generate photon pairs at a certain wavelength set ω_s (signal) and ω_i (idler). In the cascaded process, first, the pump at ω_p is up-converted to the second harmonic ($\omega_p + \omega_p \rightarrow \omega_{SH}$), and then the second harmonic (SH) photons are down-converted through SPDC: $\omega_{SH} \rightarrow \omega_s + \omega_i$. The direct process generates photon pairs through SFWM: $2\omega_p \rightarrow \omega_s + \omega_i$. The cascaded process is commonly considered to be stronger compared to the direct one. However, its phase-matching condition is more restrictive than that of the direct process.

In this work, we show that in a thin nonlinear layer, the direct process is always stronger. To demonstrate this effect experimentally, we use a 10 μm -thick lithium niobate (LN) crystal and generate photon pairs through SFWM.

2. EXPERIMENTAL SETUP

For the photon pair measurement, we use a Hanbury Brown-Twiss setup separating the entangled photon in two arms. Figure 1 shows the scheme of the experimental setup. A laser at

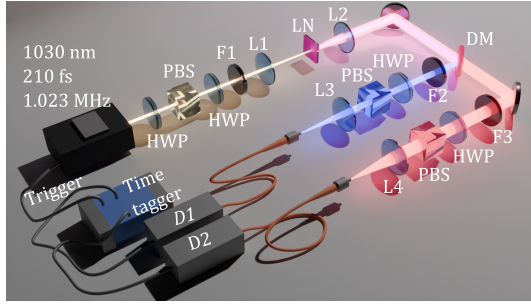


Fig. 1. Experimental setup: lens L1 focuses the pump on the LN sample; signal (visible, shown in blue) and idler (IR, shown in orange) photons are collimated by lens L2, separated by dichroic mirror DM, and coupled into detectors D1, D2 by lenses L3, L4, respectively. Their polarization is analyzed by an HWP and a PBS in each arm. Filter F1 eliminates unwanted wavelengths in the pump beam, and bandpass filters F2, F3 select the signal and idler photon detection bands. Photon detection events are registered by a time tagger triggered by pulses from the laser.

1030 nm, with a pulse duration of 210 fs and a repetition rate of 1.023 MHz, is used as the pump. Its power and polarization are controlled by two half-wave plates (HWPs) and a polarizing beam splitter (PBS). A band-pass filter (F1) at 1030 nm with 10 nm bandwidth filters out unwanted wavelengths. The pump is focused by lens L1 into a 100 μm spot on the 10 μm -thick x-cut LN layer on a 500 μm -thick fused silica substrate, and the output photons are collimated by lens L2 with the focal length 100 mm and NA=0.5. The collected photons are separated by a long-pass dichroic mirror (DM) with the cut-off wavelength at 950 nm. The visible (reflected) and IR (transmitted) photons are coupled to the multi-mode fibers at the end of each arm by lenses L3 and L4, respectively. At each arm, an HWP and a PBS are installed to analyze the polarization of the photons. The detection wavelengths are selected by band-pass filters F2 (770 nm with 10 nm band width) and F3 (1550 nm with 50 nm band width), respectively. The coupled photons are sent to single-photon detectors D1 (Perkin&Elmer, SPCM-AQRH-16-FC) and D2 (IDQ, ID220),

respectively. The detection events are triggered by the electric pulses of the laser and registered by the time tagger.

3. EXPERIMENTAL RESULTS

Figure 2 shows the experimental results. The pump power dependences of the mean photon numbers per pulse for visible and IR photons, $\langle N_{vis} \rangle$ and $\langle N_{IR} \rangle$, are plotted in panel (a) with blue circles and red triangles, respectively. The visible and IR photons

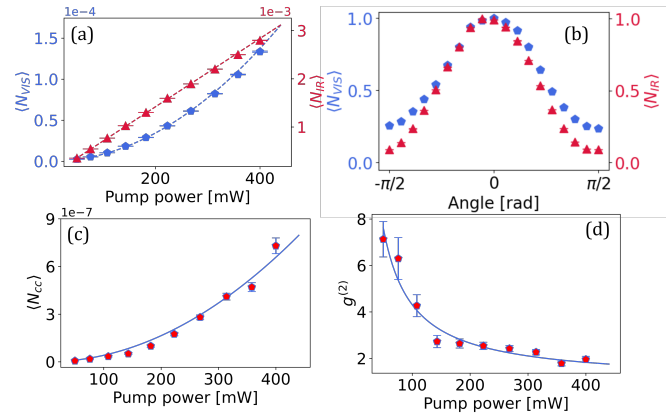


Fig. 2. SFWM in LN. (a) Mean photon number per pulse for visible (blue circles) and IR (red triangles) photons. (b) The polarization dependences of the photon detection rates in the visible (blue circles) and IR (red triangles) arms. The 0 angle corresponds to the pump polarization direction. (c) The number of coincidence counts per pulse as a function of the pump power, with a quadratic fitting curve. (d) Corresponding $g^{(2)}$ as a function of the pump power, with a fitting curve.

exhibit different dependences on the pump power, one quadratic and the other linear. The quadratic power dependence is indeed expected for SFWM. Meanwhile, the linear power scaling of the IR photons rate with the pump can be explained by SPDC. Indeed, under pumping at 1030 nm, SPDC in thin LN can generate signal photons at 1550 nm, with their idler counterparts being at 3.078 μm . The coherence length for this process is 15 μm , longer than the sample thickness. While the idler photons cannot be detected by our setup, the signal photons generation rate should be much higher than the SFWM rate. Consequently, the dominant contribution to the rate of IR photons is from SPDC, which scales linearly with the pump power. Importantly, SPDC cannot affect the coincidence detection in our experiment because the idler SPDC photons are not detected in the visible arm.

Since the strongest components of LN second- and third-order nonlinear susceptibility tensors are $\chi_{zzz}^{(2)}$ and $\chi_{zzzz}^{(3)}$, respectively, both SPDC and SFWM are most efficient if the pump and the output photons are all polarized along the z axis. Indeed, the photon count rates are maximal for the pump polarized along the z axis (see Supplement 1). Also, from Fig. 2(b), where the polarization dependences of $\langle N_{vis} \rangle$ and $\langle N_{IR} \rangle$ are plotted, we see that both visible and IR photons are polarized the same way as the pump. For visible photons, this is evidence that they mostly come from SFWM and not from two-photon photoluminescence.

Figure 2(c) shows the mean number of coincidences per pulse $\langle N_{cc} \rangle$ as a function of the pump power. The dependence is quadratic, as expected for SFWM. The efficiency of pair generation is much lower than the one measured in SiN films using

the same pump [24]; however, higher rates can be achieved because of the high damage threshold of LN at 1030 nm. The second-order correlation function $g^{(2)}$, calculated as

$$g^{(2)}(0) = \frac{\langle N_{cc} \rangle}{\langle N_{vis} \rangle \langle N_{IR} \rangle}, \quad (1)$$

is plotted in panel (d). The fitting curve is $g^{(2)} = 1 + a/P^2$, where a is a fitting parameter and P is the pump power. The $g^{(2)}$ exceeding the 'thermal' value 2 and its inverse dependence on the mean photon number of SFWM (scaling as P^2) indicate the detection of correlated photon pairs.

Importantly, the fused silica substrate could also contribute to SFWM, due to its noticeable $\chi^{(3)} = 3 \times 10^{-22} \text{ m}^2/\text{V}^2$ [27] and large length. Its contribution can be estimated from these parameters and the phase matching condition (see the Supplementary Information) as 25% of the total rate of coincidences.

So far, it was not clear if the observed photon pairs are generated through the direct or cascaded process. To figure out the contribution of the cascaded process, we first investigated the efficiency of its second stage. To this end, using the same setup, we detected photon pairs from SPDC pumped at 515 nm. The pump was prepared by frequency-doubling the 1030 nm radiation in a bulk phase-matched BBO crystal installed after F1 (see Fig. 1). Further, knowing the efficiency of SHG from the LN layer, we estimated $\langle N_{cc} \rangle$ stemming from the cascaded process.

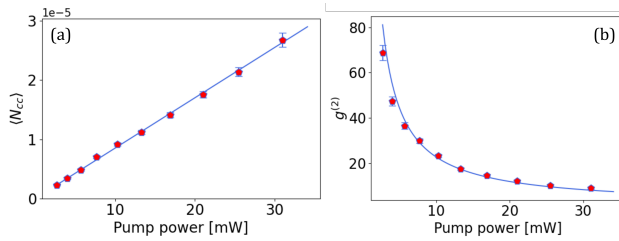


Fig. 3. SPDC in LN pumped at 515 nm. (a) The mean number of coincidence counts per pulse as a function of the pump power, with a linear fit. (b) Corresponding $g^{(2)}$ as a function of the pump power, with the fitting curve.

Figure 3 shows the correlation measurement results for SPDC in the same LN layer, pumped at 515 nm. The mean number of coincidences per pulse $\langle N_{cc} \rangle$ is plotted as a function of pump power with a linear fitting curve in panel (a). Panel (b) shows the correlation function $g^{(2)}$, calculated according to Eq. 1, with the fitting curve $g^{(2)} = 1 + a/P$. Meanwhile, the SHG efficiency of the LN layer is evaluated by measuring the pump and SH powers after the sample. The measured conversion efficiency is $2 \times 10^{-22} \text{ W}^{-1}$: pumping with 400 mW at 1030 nm yields 30 μW of SH. Based on this measurement, under 400 mW pumping the cascaded process generates 4×10^{-8} pairs per pulse, which is only 5% of the total rate of photon pairs.

4. ANALYSIS AND DISCUSSION

To describe the cascaded and direct processes theoretically, consider first their phase-matching functions

$$F(L) = L \text{sinc} \frac{\Delta k L}{2}, \quad (2)$$

where Δk is the wavevector mismatch and L the crystal length. Figure 4 shows $[F(L)]^2$ for each of the three involved processes:

SFWM generating 770 nm / 1550 nm photon pairs from 1030 nm pump (green solid line), SHG from 1030 nm (blue dot-dashed line), and SPDC generating 770 nm / 1550 nm photon pairs from 515 nm pump (red dashed line). For each process, the phase matching function oscillates (Maker fringes), reaching maxima at odd numbers of the nonlinear coherence length $L_{coh} = \pi/|\Delta k|$. The nonlinear coherence lengths for the three processes are 33.3 μm , 3.1 μm , and 3.4 μm , respectively; therefore, the efficiencies of both steps of the cascaded process should oscillate faster than the efficiency of direct SFWM. Moreover, because the peak values of $F^2(L)$ scale inversely with Δk^2 , they are much lower for SHG and SPDC than for SFWM. This already gives a qualitative explanation for the effect we see: because $|\Delta k_{SFWM}| = |\Delta k_{SHG}| - |\Delta k_{SPDC}| \ll |\Delta k_{SHG}|, |\Delta k_{SPDC}|$, the phase-matching function of SFWM considerably exceeds the ones of SHG and SPDC.

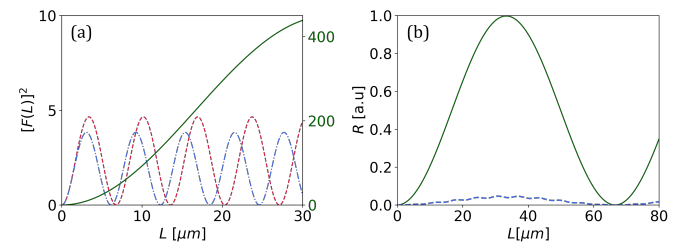


Fig. 4. (a) $[F(L)]^2$ calculated for SFWM generating 770 nm / 1550 nm photon pairs from 1030 nm pump (green solid line), SHG from 1030 nm (blue dot-dashed line), and SPDC generating 770 nm / 1550 nm photon pairs from 515 nm pump (red dashed line) as functions of the crystal length. (b) Calculated rates of photon pair generation through the direct (green) and cascaded (blue dashed line) processes vs the crystal length.

For an accurate comparison, we consider both second-order processes, SHG and SPDC, occurring simultaneously. Assuming a non-depleted pump, the electric field amplitude of the SH generated from the pump propagating along the x -direction is [27]

$$E_{SH}(x) = \frac{2\pi}{\lambda_{SH}} \chi_{SHG}^{(2)} E_p^2 \frac{e^{i\Delta k_{SHG} \cdot x} - 1}{\Delta k_{SHG}}, \quad (3)$$

where λ_{SH} , E_p , and $\chi_{SHG}^{(2)}$ are the SH wavelength, the amplitude of pump field, and the effective second-order nonlinear susceptibility for SHG, respectively. The Hamiltonian of SPDC generating photons at frequencies ω_s and ω_i from the SH is [28]

$$\hat{H}_{SPDC} = \frac{2}{3} C(\omega_s, \omega_i) \int_0^L dx \cdot \chi_{SPDC}^{(2)} E_{SH}(x) e^{i\Delta k_{SPDC} \cdot x} a_s^\dagger a_i^\dagger + H.c., \quad (4)$$

where $a_{s,i}^\dagger$ are the creation operators for the signal and idler photons, $H.c.$ means Hermitian conjugation, $\chi_{SPDC}^{(2)}$ is the effective second-order nonlinear susceptibility for SPDC, and we have introduced $C(\omega_s, \omega_i) \equiv \hbar \sqrt{\omega_s \omega_i} / (2\epsilon_0 V_q n_s n_i)$, with $n_{s,i}$ being the refractive indices at signal and idler wavelengths and V_q the quantization volume. By substituting Eq. (3) into Eq. (4) and integrating, we get the Hamiltonian of the cascaded process in the form

$$\hat{H}_{cas} = \frac{2}{3} C(\omega_s, \omega_i) A_{cas} a_s^\dagger a_i^\dagger + H.c., \quad (5)$$

with the amplitude

$$A_{cas} = \frac{2\pi[\chi^{(2)}]^2 E_p^2}{n_{SH}\lambda_{SH}\Delta k_{SHG}} e^{i\Delta k_{SPDC}L/2} \times [e^{i\Delta k_{SHG}L/2} F_{SFWM}(L) - F_{SPDC}(L)], \quad (6)$$

where n_{SH} is the refractive index at λ_{SH} , and we assumed $\chi_{SPDC}^{(2)} = \chi_{SHG}^{(2)} \equiv \chi^{(2)}$ and used the relation $\Delta k_{SFWM} = \Delta k_{SHG} + \Delta k_{SPDC}$.

Meanwhile, the Hamiltonian for direct SFWM is [29, 30]

$$\hat{H}_{dir} = \frac{3}{4}C(\omega_s, \omega_i) \int_0^L dx \chi_{SFWM}^{(3)} E_p^2 e^{i\Delta k_{SFWM}x} a_s^\dagger a_i^\dagger + H.c = \frac{3}{4}C(\omega_s, \omega_i) A_{dir} a_s^\dagger a_i^\dagger + H.c, \quad (7)$$

with the amplitude

$$A_{dir} = \chi_{SFWM}^{(3)} E_p^2 e^{i\Delta k_{SFWM}L/2} F_{SFWM}(L). \quad (8)$$

Omitting the common factors in Eqs. (5,7), we see that the rates of pair generation through the cascaded and direct processes are, respectively, $R_{cas} \propto \frac{4}{9}|A_{cas}|^2$ and $R_{dir} \propto \frac{9}{16}|A_{dir}|^2$.

Figure 4 (b) shows these rates as functions of the crystal length: in green solid line for the direct process and in blue dot-dashed line for the cascaded process. For the calculation, we used the values of $\chi^{(2)} = 2.5 \times 10^{-11} \text{ m/V}$ [31] and $\chi_{SFWM}^{(3)} = 1.5 \times 10^{-20} \text{ m}^2/\text{V}^2$ [32]. The rates oscillate with the same period, equal to twice the coherence length of the SFWM process. This is because the first term in the square brackets of Eq. (6) dominates, see Fig. 4(b). At 10 μm thickness, the ratio R_{cas}/R_{dir} is 0.048, which is in good correspondence to the experimental result.

If the cascaded process has the phase matching satisfied for both its stages (i.e., through periodic poling), it should be more efficient than direct SFWM. Note that for $\Delta k_{SH} = \Delta k_{SPDC} = 0$, the field in Eq. (3) scales as z , which leads to Eq. (6) scaling as L^2 instead of L . But here we see that without phase matching satisfied, SHG and SPDC have larger wavevector mismatches than SPDC, which makes the cascaded process less efficient than the direct one.

SFWM in thin second-order nonlinear films can considerably enrich the toolbox of 'flat' quantum optics. In high- $\chi^{(2)}$ semiconductors, such as GaAs or AlGaAs, it can produce photon pairs with one of the photons above the bandgap, which is impossible through SPDC. Moreover, as we show above, a second-order nonlinear film pumped at frequency ω_p can simultaneously generate photon pairs at frequencies ω_s and ω_i through SFWM, but also at frequencies ω_i and $\omega_p - \omega_i$ through SPDC. This simultaneous action of two coherently pumped nonlinear effects can be used for building interesting quantum superpositions.

5. BACK MATTER

Funding. Deutsche Forschungsgemeinschaft (568143457); ERC (Project 101199215 — MultiFlaQS).

Acknowledgment. We thank Francesco Tani, who kindly allowed us to use his laser.

Disclosures. The authors declare no conflicts of interest.

Data Availability. Data underlying the results presented in this paper are not publicly available at this time but may be obtained from the authors upon reasonable request.

Supplemental document. See Supplement 1 for supporting content.

6. REFERENCES

REFERENCES

1. C. Okoth, A. Cavanna, T. Santiago-Cruz, and M. V. Chekhova, *Phys. review letters* **123**, 263602 (2019).
2. T. Santiago-Cruz, V. Sultanov, H. Zhang, *et al.*, *Opt. Lett.* **46**, 653 (2021).
3. V. Sultanov, T. Santiago-Cruz, and M. V. Chekhova, *Opt. Lett.* **47**, 3872 (2022).
4. Q. Guo, X.-Z. Qi, L. Zhang, *et al.*, *Nature* **613**, 53 (2023).
5. V. Sultanov and M. Chekhova, *ACS photonics* **11**, 2 (2023).
6. M. A. Weissflog, A. Fedotova, Y. Tang, *et al.*, *Nat. Commun.* **15**, 7600 (2024).
7. E. A. Santos, M. A. Weissflog, T. Pertsch, *et al.*, *Nanophotonics* **13**, 3545 (2024).
8. J. Feng, Y.-K. Wu, R. Duan, *et al.*, *eLight* **4**, 16 (2024).
9. X. Lyu, L. Kallioniemi, H. Hong, *et al.*, *Nat. Commun.* **16**, 1899 (2025).
10. H. Liang, T. Gu, Y. Lou, *et al.*, *Sci. Adv.* **11**, eadit3710 (2025).
11. N. J. Sørensen, V. Sultanov, and M. V. Chekhova, *Opt. Express* **33**, 13946 (2025).
12. S. Stich, V. Sultanov, T. Blaikie, *et al.*, *Opt. Express* **34**, 1664 (2026).
13. V. Sultanov, A. Kavčič, E. Kokkinakis, *et al.*, *Nature* **631**, 294 (2024).
14. Z. Lu, J. Janousek, S. M. Assad, *et al.*, *Nat. Commun.* **16**, 9616 (2025).
15. A. Säynätjoki, L. Karvonen, H. Rostami, *et al.*, *Nat. Commun.* **8**, 893 (2017).
16. S. Klopčič, A. Kavčič, N. Sebastián, and M. Humar, *Adv. Sci.* **n/a**, e15206 (2025).
17. S. Lopez-Huidobro, M. Noureddin, M. V. Chekhova, and N. Y. Joly, *Opt. Lett.* **48**, 3423 (2023).
18. L. Caspani, R. Kaipurath, M. Clerici, *et al.*, *Phys. review letters* **116**, 233901 (2016).
19. E. G. Carnemolla, W. Jaffray, M. Clerici, *et al.*, *Opt. Lett.* **46**, 5433 (2021).
20. L. Xu, D. A. Smirnova, R. Camacho-Morales, *et al.*, *New J. Phys.* **24**, 035002 (2022).
21. J. Yang, X. Xiao, J. Flórez, *et al.*, *ACS Photonics* **12**, 4415 (2025).
22. S. C. Malek, T. Norden, C. F. Doiron, *et al.*, *ACS nano* **19**, 35609 (2025).
23. K. F. Lee, Y. Tian, H. Yang, *et al.*, *Adv. Mater.* **29**, 1605978 (2017).
24. C. Son, S. Peana, O. Matthiessen, *et al.*, *Opt. Lett.* **50**, 4434 (2025).
25. S. D. Gennaro, C. F. Doiron, N. Karl, *et al.*, *ACS Photonics* **9**, 1026 (2022).
26. S. M. Saltiel, A. A. Sukhorukov, and Y. S. Kivshar, "Multistep parametric processes in nonlinear optics," in *Progress in optics*, , vol. 47 (Elsevier, 2005), pp. 1–73.
27. R. Boyd, *Nonlinear Optics* (Academic Press, 1992).
28. M. H. Rubin, D. N. Klyshko, Y. Shih, and A. Sergienko, *Phys. Rev. A* **50**, 5122 (1994).
29. L. Wang, C. Hong, and S. Friberg, *J. optics B: Quantum semiclassical optics* **3**, 346 (2001).
30. K. Garay-Palmett, A. B. U'Ren, and R. Rangel-Rojo, *Phys. Rev. A* **82**, 043809 (2010).
31. I. Shoji, T. Kondo, A. Kitamoto, *et al.*, *J. Opt. Soc. Am. B* **14**, 2268 (1997).
32. Y. Wang, Y. Niu, G. Wang, *et al.*, *J. Alloy. Compd.* **778**, 691 (2019).